4.1. Introduction

Bismuth lanthanum titanate, $Bi_3LaTi_3O_{12}$ (BLTO) was showing the great interest in research of ferroelectric materials due to their technological application in sensors, actuators and nonvolatile random access memories (NRAM) ferroelectric. Lead-based ferroelectric materials such as $Pb(Zr,Ti)O_3$ (PZT) were the most widely used piezoelectric materials because of their better electrical properties [B. Jaffe, W.R. Cook, H. Jaffe (2017)]. The high remnant polarization of PZT at low temperature made it a dominant material for memory devices presently being used in ferroelectric random access memory (FRAM) [J. F. Scott, CA Pas de Araujo (1989), Zhang *et al.* (2003)]. However, these materials have shown drawbacks of fatigue, leakage current and aging [Zhang *et al.* (1994), Warren *et al.* (1995)]. Additionally, PZT has high lead content. The evaporation of toxic lead during fabrication of the ceramics may cause the major health and environment problems in the long term. In addition, there is also a desire to restrictions the integration of lead containing materials in to electronic devices, the bismuth based layered ferroelectrics are environment friendly. Lead-free bismuth layer-structured ferroelectric thin films, such as $SrBi_2Ta_2O_9$ (SBT) and $Bi_4Ti_3O_{12}$ (BTO) have been confined in the usual industrial application due to its small polarization and high processing temperature [Lettieri *et al.* (2000), Lee *et al.* (2000)]**.** BTO has been copiously studied because of their better strain resistance on common Pt electrodes [Park *et al.* (1999)] and large spontaneous polarization (P_s), low processing temperature and high Curie temperature ($T_c = 675$ °C) [Liu *et al.* (2010)]. Its layered structure belongs to the Aurivillius family having desirable electrical and electromechanical properties [Fang *et al.* (2012), Ahn *et al.* (2009), Subbarao *et al.* (1962)]. Furthermore, there is a rising the demand to succeed the lead based material and develop a new lead free material. La doped BTO exhibited low processing temperature and large value of remnant polarization [Kojima *et al.*

(2001), Pavlović *et al.* (2011), Rachna *et al.* (2010)].It is also significant with Si-based integrated circuit technology.

In the past, few literature of BLTO compound mostly explains thin film and ferroelectric behavior but in this manuscript, we have synthesized BLTO ceramic first time fabricated via semi wet route at low temperature. This method has many advantages than other methods such as conventional solid state method and sol-gel methods because this method is simple and carries out using metal nitrate solutions and solid TiO_2. It is simpler as compared to the solid state method because solid state method contains several multi-steps (i.e; intermediate grindings, drying, etc.) to get precursor powder. On the other hand, in the case of sol-gel methods a very costly alkoxide of titanium is used as Titanium source. In the present work, we have used the cheap solid TiO_2 as Titanium source which was directly added to the metal nitrate solution to get BLTO precursor powder on combustion. This fabrication route shows the enhancement of dielectric and magnetic properties. The aim of the present work is to examine the dielectric and magnetic behavior of the $Bi_3LaTi_3O_{12}$ ceramic fabricated by semi-wet route. The ceramic has been characterized by various techniques, XRD, TEM, SEM and AFM analysis.

4.2. Experimental

$Bi_3LaTi_3O_{12}$ceramic was fabricated by the semi-wet route. The analytical grade chemicals of Bismuth nitrate, $Bi(NO_3)_3.5H_2O$ (99.5%, Merck, India), Lanthanum oxide, La_2O_3 (99.0%; Merck, India), titanium oxide, TiO_2 (99.9%, Merck, India) were taken in stoichiometric ratio. The solutions of $Bi(NO_3)_3.5H_2O$ was prepared using distilled water and La_2O_3 dissolved in dilute nitric acid. Both the solutions were mixed in a beaker. The solid TiO_2 in form of powder was added to the solution.

A calculated amount of citric acid equivalent to the metal ions was dissolved in water and added in the heterogeneous mixture. The resultant heterogeneous mixture was heated on a hot plate using magnetic stirrer at 70-80 ℃ to evaporate water. The residual mass was dried at 100-120 ℃ in hot air oven. The BLTO dried powder was calcined at 800 ℃ for 6 h in a muffle furnace and ground into a fine powder using poly vinyl alcohol (PVA) as a binder in a mortar and pestle. Cylindrical pellets (11.6 mm x 1.00 mm) were made using a hydraulic press. The pellets were sintered at 900 ℃ for 8 h.

The crystalline phase of sintered sample was identified by X-ray diffractometer (Rigaku Miniflex 600, Japan) using CuK$_\alpha$ as X-ray source with a wavelength of 1.54 Å. The FT-IR spectra of calcined powder of BLTO ceramic was recorded by an ATR-FTIR spectrophotometer (Bruker, ALPHA model) in the range from 4000 - 500 cm^{-1}. The bright field TEM image of the ceramic was examined using a transmission electron microscope (TEM, FEI TECANI G^2 20 TWIN, U.S.A.). The microstructure of the fractured surfaces of pellet was examined by using a scanning electron microscope (ZEISS, model EVO-18 research, Germany). The elemental analysis of the sintered sample of BLTO was performed by EDX (Oxford instrument; U.S.A.) attached with the SEM unit. The surface morphology and roughness of BLTO ceramic were examined using atomic force microscopy (NTEGRA Prima, Germany). Temperature and field-dependent dc magnetization of ceramic were measuredby using Magnetic Property Measurement System Quantum Design MPMS-3, over a temperature range 2–300 K at a magnetic field of ±7 tesla. The temperature variation of field cooled (FC) and zero field cooled (ZFC) magnetization at 100 Oe applied field were carried out using SQUID VSM dc magnetometer. The dielectric data of BLTO ceramic pellets coated with silver paints were collected using the LCR meter (PSM 1735, Newton

4[th]Ltd, U.K.) with the variation of frequency (100 Hz – 5 MHz) and temperature (300-500 K).

4.3. Results and discussion

4.3.1. Microstructural studies

Fig.4.1 displayed XRD patterns of BLTO calcined at 800 ℃ for 6 h and sintered pellet at 900 ℃ for 8 h.
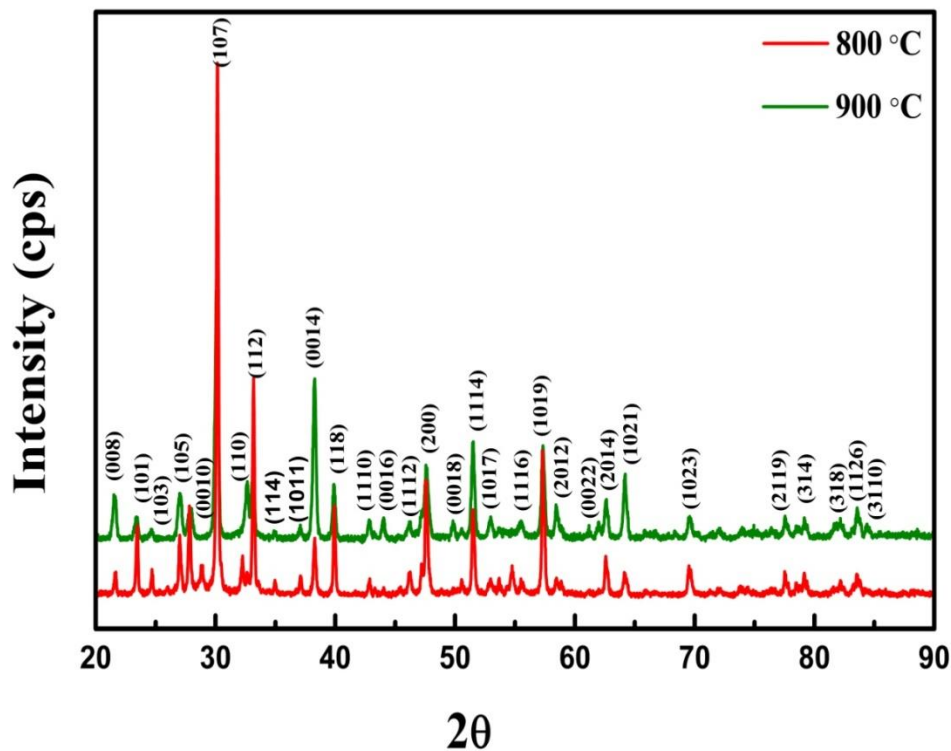

Fig.4.1. XRD patterns of BLTO ceramic (a) calcined at 800 °C for 6 h and (b) sintered at 900 °C for 8 h.

XRD pattern of calcined powder and sintered pellets are identical to each other which reveal the same phases. On analysis the XRD peaks, it was observed the single phase formation of $Bi_4Ti_3O_{12}$ as per JCPDS card No. 89-7503.

Fig.4.2 shows the Fourier transform infrared (FTIR) spectrum of BLTO calcined powder at 800 °C for 6 h. The most of the citrate group disappears during the combustion process. The peaks observed at 410, 592 and 836 cm^{-1} for the calcined powder were due to bending and stretching mode of Ti-O-Ti and Ti-O band [Devi *et al.* (2014), Gautam *et al.* (2016)].
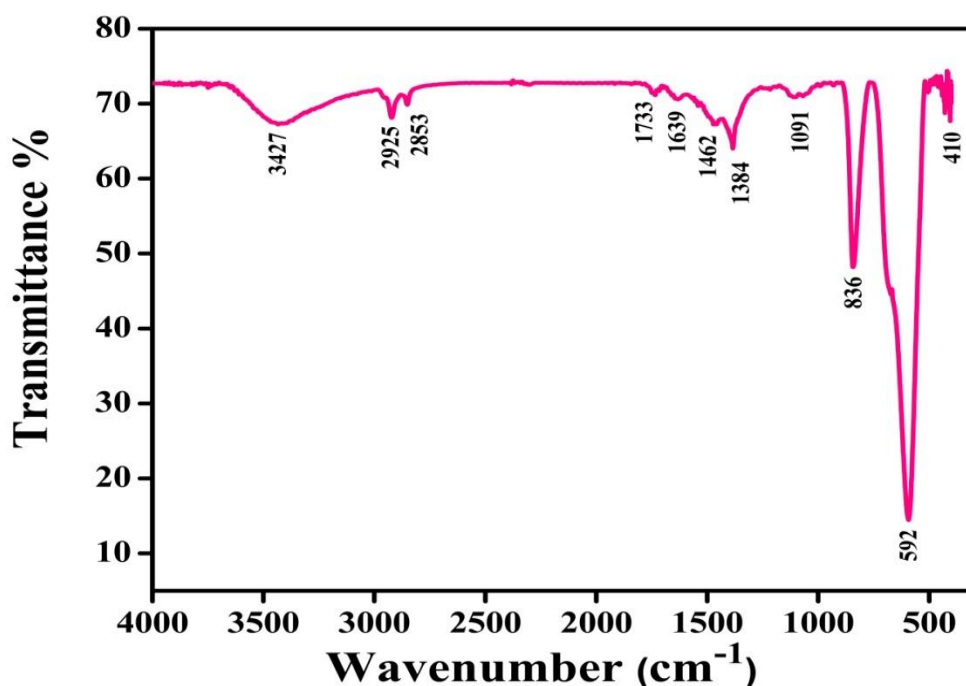

Fig.4.2. FITR spectra for the BLTO ceramic calcined at 800 °C for 6 h.

The peak observed at 1639 cm^{-1} could be assigned to the OH vibrational mode of the absorbed water molecule [Ocwelwang *et al.* (2014)].

Mostly band characteristics of oxygen–metal bonds were exhibited in the 400–850 cm^{-1} [Simoes *et al.* (2006), He *et al.* (2014)]. Fig. 4.3(a) shows transmission electron microscopy (TEM) bright field images of the BLTO ceramic. The shape of the particle was found to be spherical and platelet like. The average particle size was found to be in the ranges of 212 ± 20 nm. The average particle size calculated from the XRD peak proves the result exhibited by TEM analysis.
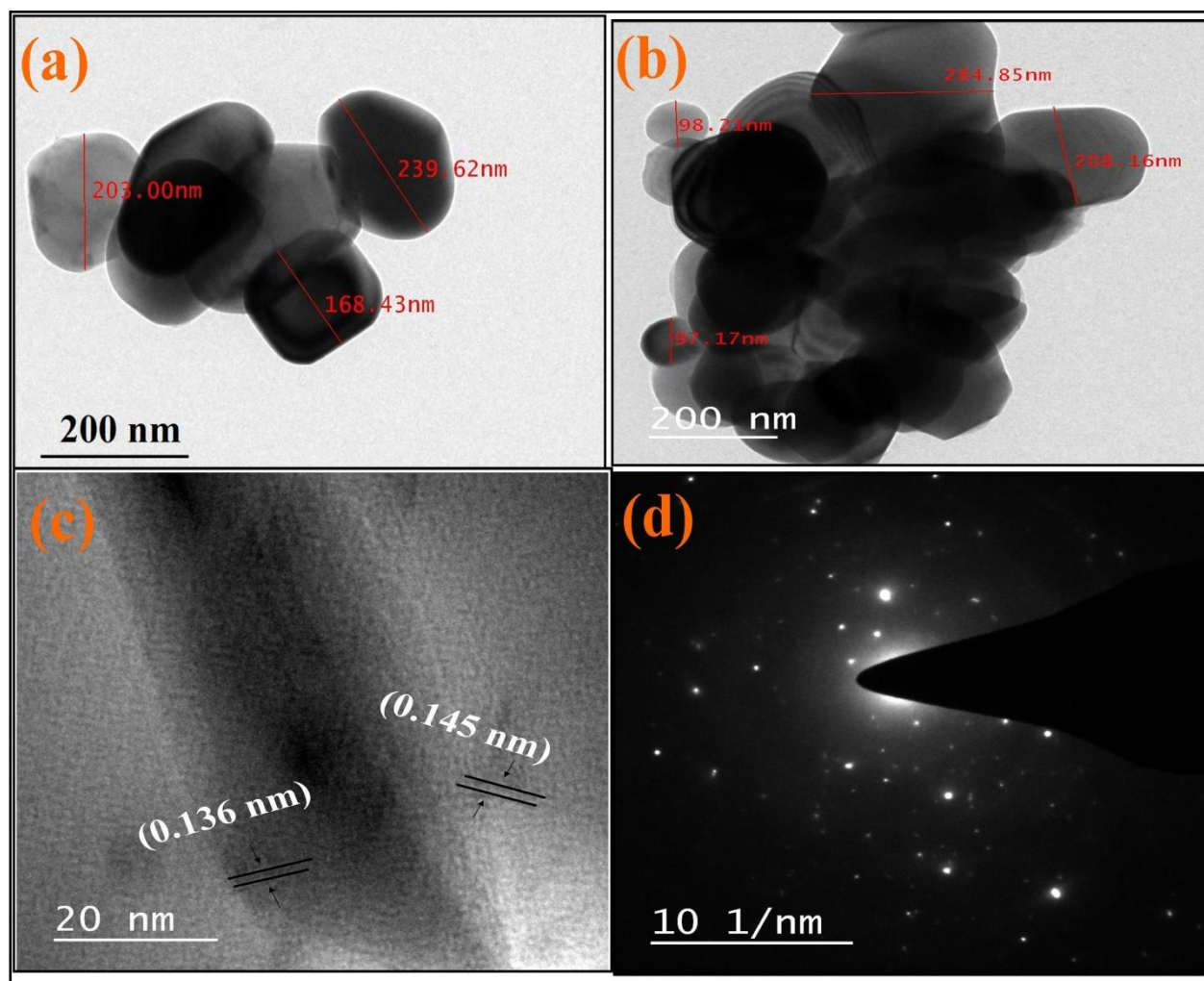

Fig.4.3.(a & b) shows TEM micrographs of BLTO ceramic sintered at 900 °C for 8 h, (c) presents a high resolution TEM micrograph of the BLTO interface and (d) SAED pattern of BLTO ceramic.

Fig. 4.3(c) shows the high-resolution TEM analysis (HRTEM) of BLTO ceramic. In this figure, distinct parallel lines indicated inter-planer distance (d). The values of d were found to be 0.136 and 0.145 nm matched with a plane (222) and (2 0 16) of BLTO ceramic respectively. These result also supported by XRD study. Fig. 4.3(d) shows the selected area electron diffraction (SAED) of BLTO ceramic. The presence of spot patterns in the SAED supporting the formation of nano ceramic.
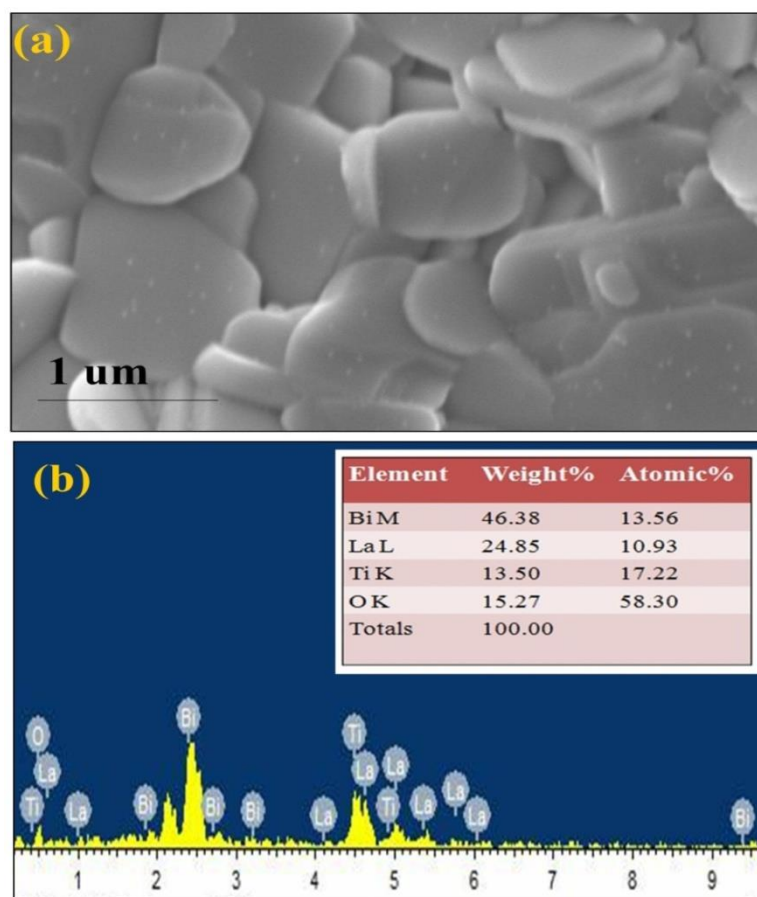
Element	Weight%	Atomic%
Bi M	46.38	13.56
La L	24.85	10.93
Ti K	13.50	17.22
O K	15.27	58.30
Totals	100.00	

Fig.4.4. (a) SEM image (b) the corresponding EDX spectrum of Bi₃LaTi₃O₁₂ ceramic sintered at 900 °C for 8 h.

Fig.4.4 (a) shows microstructure of the fracture surface observed from the scanning electron microscopy. The SEM image exhibits flake like and platelet type bimodal grains [Roy *et al.* (2011)]**.** The average grain size of the BLTO ceramic was found to be in the range of 200 ± 20 nm. The EDX spectrum of BLTO ceramic was confirmed the presence of elemental compositions showing in Fig. 4.4(b). The atomic percentages of Bi, La, Ti and O, were found to be 13.56, 10.93, 17.22 and 58.30, respectively showing the inset figure 4.4(b).
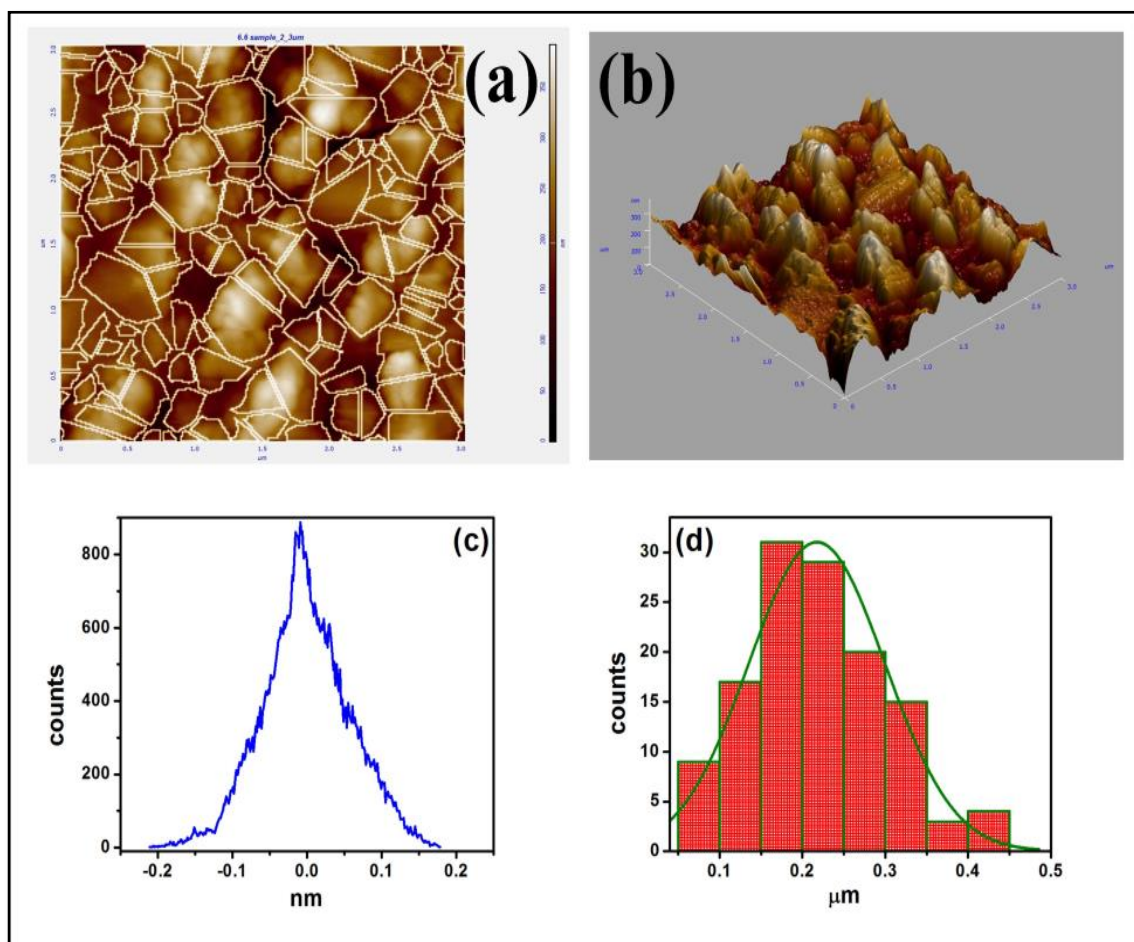

Fig.4.5. AFM images of BLTO ceramic sintered at 900 °C for 8 h (a) two-dimensional and corresponding watershed image showing grains and grain boundaries (b) three-dimensional image exhibited high peak distribution (c) histogram of three-dimensional particle roughness and (d) particle size distribution curve.

These results clearly show the presence of Bi, La, Ti and O as per the stoichiometric ratio in BLTO ceramics which confirmed the purity of the material [Singh *et al.* (2013), Prakash *et al.* (2007)]. The AFM image of BLTO ceramic shows the surface morphology of grains and grain boundary for a two-dimensional image in Fig. 4.5(a). It exhibited compact structure with granular morphology with clear grain boundary. Fig. 4.5(b) shows three-dimensional AFM image which indicates the maximum area peak height of the grain to be 179.98 nm within the scan area of 3.0 μm × 3.0 μm. Fig. 4.5(c) shows the three-dimensional surface roughness of BLTO ceramic. The average roughness and root mean square roughness of the ceramic were found to be 46.015 nm and 58.661 nm, respectively. The AFM analysis revealed the presence of the particles with the broad size distribution in the BLTO ceramic [Gautam *et al.* (2017)]. The average grain size estimated for two-dimensional was found to be 217 ± 20 nm out of 128 grains as shown in the histogram Fig. 4.5(d). The result of TEM, SEM and AFM analysis always supports to each other.

4.3.2. Magnetic studies

Fig.4.6 (a) shows the magnetization behavior of BLTO ceramic as a function of temperature. The hysteresis curve of zero-field cooling (ZFC) and field cooling (FC) measured in the temperature range 2-300 K at the applied field of 100 Oe. The ZFC shows a cups and bifurcation with the corresponding to FC curve below 300 K. It was typically present in a gathering of ferromagnetic like particle exhibiting super magnetic above a certain temperature. The cups in ZFC curve defined the blocking temperature [Chu *et al.* (2014)]. The blocking temperature is found to be 155 K. On the other hand, the FC curve shows hump like a minor peak at 51 K. the temperature knows as Neel's temperature. It appears to be an anti-ferromagnetic and ferromagnetic moment. The ceramic shows both

type behavior, blocking temperature and Neel's temperature of ZFC and FC curve by bimodal size distribution corresponding to TEM images. The large particle explains to Neel's temperature and blocking for the smaller particle size [Mendonça *et al.* (2012)]. Fig. 4.6(b) shows the magnetization as a function of magnetic field measured at 7 T for the BLTO ceramic.
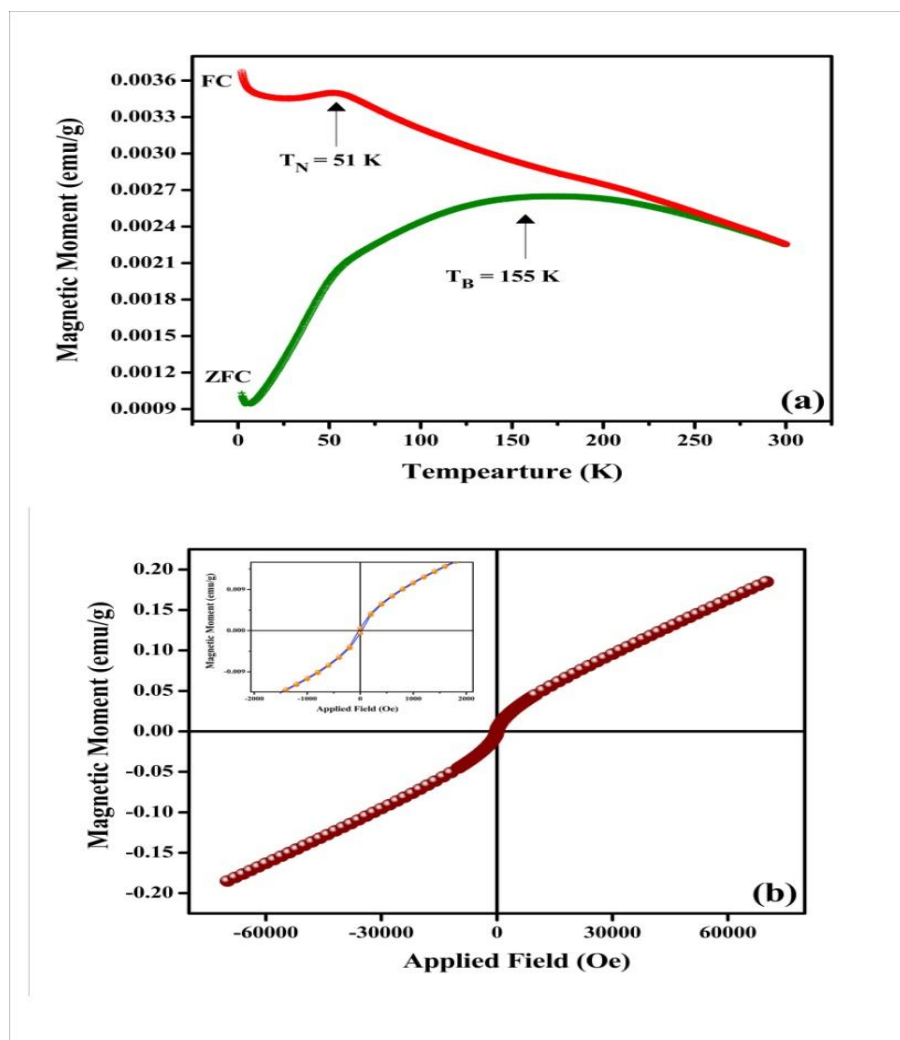

Fig.4.6.(a) Temperature-dependent zero field cooled (ZFC) and field cooled (FC) magnetization measured at H = 100 Oe and (b) magnetization versus applied field at 300 K for the BLTO ceramic.

The magnetization curves show no perfect saturation and it has been situated even at a magnetic field of 7 T at room temperature. It is observed that BLTO ceramic shows anti-ferromagnetic and weak ferromagnetic in nature. The coercivity shows open hysteresis loop approximate at 72 Oe as shown in the inset of figure. The apparent opening has been exhibited in the curves indicating the existence of ferromagnetic moment. This weak ferromagnetic moment arises due to spin canting of the atomic magnetic moments and could not be compensated spin at the surface of BLTO ceramic [Mendonça *et al.* (2012), Babu *et al.* (2015)]**.**

4.3.3. Dielectric studies

Temperature dependence of the dielectric constant (ε') and loss tangent for the BLTO ceramic at few selected frequencies (100 Hz, 1 kHz, 10 kHz and 100 kHz) is shown in Figure 4.7. It is observed from the Fig.4.7 (a) that the dielectric constant of BLTO ceramic is independent of behavior up to 400 K and then increases slowly. The value of ε' was gradual decreases with increasing frequency at a given temperature. The dielectric constant of BLTO ceramic was found to be 405, 337, 211 and 153 at 100 Hz, 1 kHz, 10 kHz and 100 kHz respectively; at 500 K. Temperature dependence of loss tangent (tan δ) of the BLTO ceramic is shown in Fig. 4.7. (b). The tanδ is strongly temperature dependent and it increases with decrease in frequency. The value of tanδ is lowest (0.076) at 100 kHz and 500 K. Fig. 4.8 shows the variation of dielectric constant (ε') and loss tangent (tanδ) with frequency at few selected temperatures. It is observed from Fig. 4.8(a), the dielectric constant increases with decrease in frequency. The high value of the dielectric constant at low frequency region is due to the presence of space charge polarization in the ceramic [Chaudhuri *et al.* (2012)]**.** The low value of the dielectric constant at higher frequencies is important for the ferroelectric and electro-optic devices.
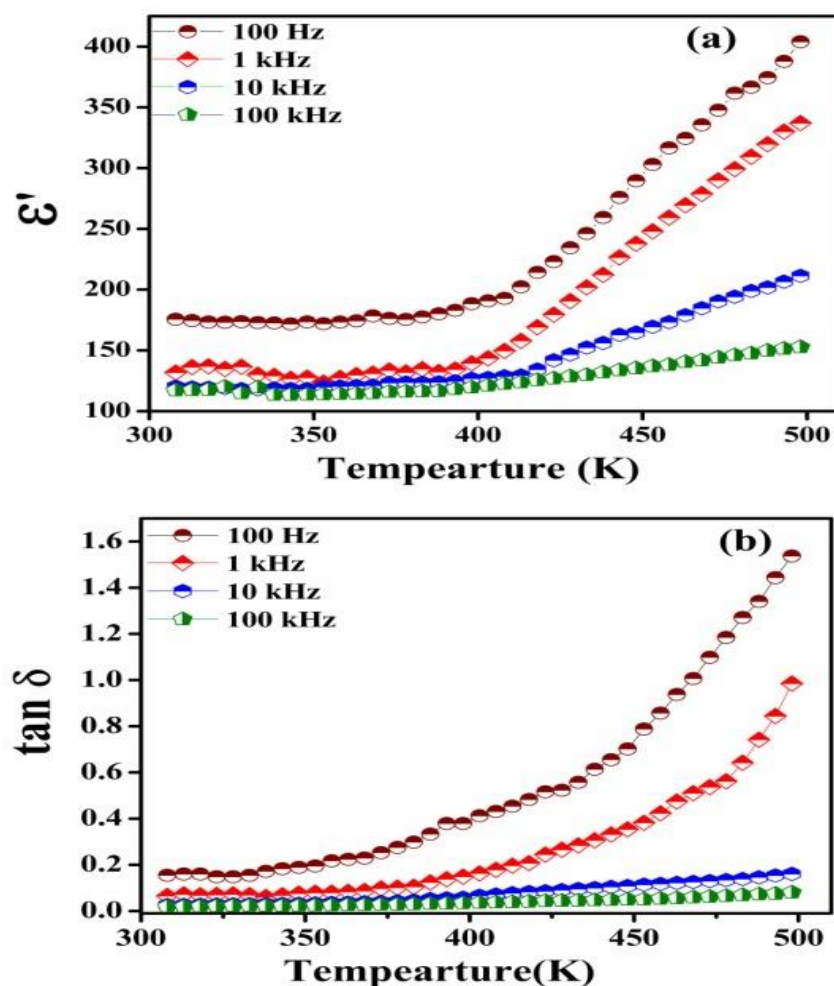
Fig.4.7. Plot of (a) dielectric constant and (b) tan δ as a function of temperature for BLTO ceramic sintered at 900 °C for 8 h.

Frequency dependent dielectric studies show the low frequency relaxation is associated with the entity of barrier layers at the electrode and the high frequency region with the entity of barrier layers at grain boundaries [Balamurugaraj *et al.* (2013), Ponpandian *et al.* (2002]. Fig. 4.8(b) shows decreases of tanδ with increasing frequency at few selected temperature. The lowest value of tan δ was found to be 0.75 at 428 K.
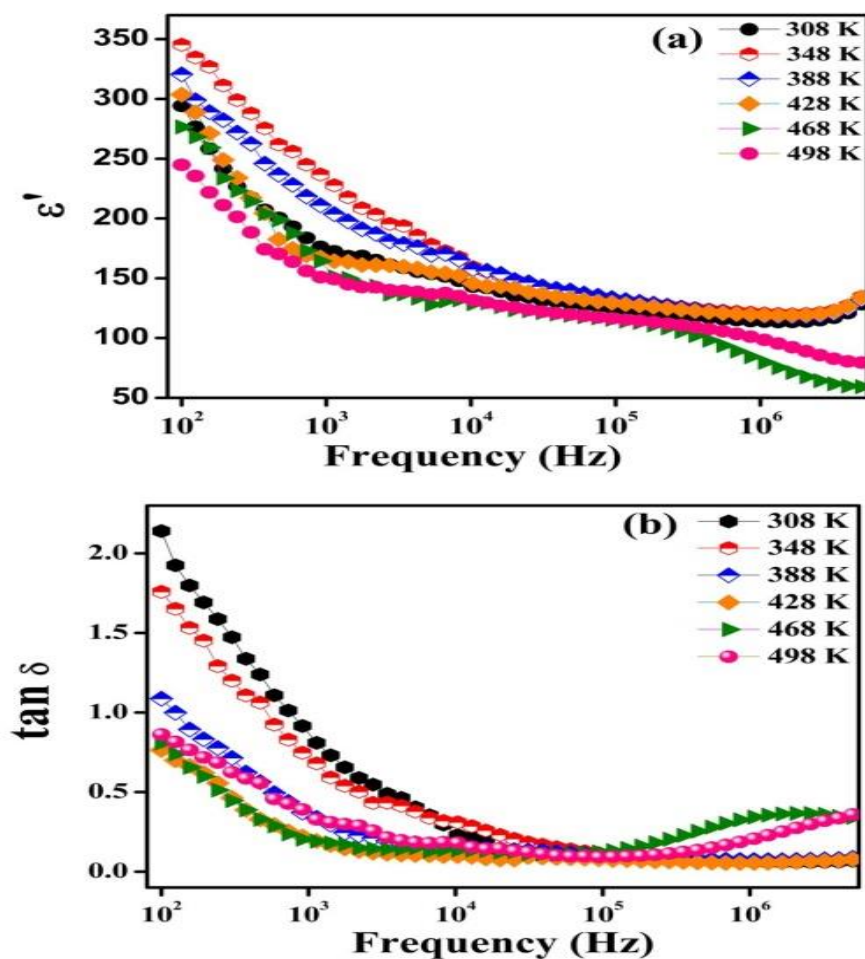
Fig.4.8. Plot of (a) dielectric constant and (b) tan δ as a function of frequency for BLTO ceramic sintered at 900 °C for 8 h.

The relaxation peaks in tanδ were observed at high frequency regions. The above characteristic behavior of a ferroelectric relaxor is usually characterized by diffuse phase transition and strong relaxational dispersion in dielectric constant and tanδ indicating the thermally activated relaxation. In both the curves, the dielectric constant and loss tangent

increases with decreasing frequency, which is the common feature of polar dielectric materials.

4.4. Conclusion

$Bi_3LaTi_3O_{12}$ ceramic was synthesized by semi-wet route at low temperature. The single phase formation of the ceramic was confirmed by XRD. The average particle size of the BLTO ceramic was found to be 212 ± 20 nm by TEM analysis. The Ti-O and Ti-O-Ti band stretching frequency were confirmed by FT-IR in the BLTO ceramic calcined at 800 °C. The SEM study of BLTO ceramic sintered at 900 °C for 8 h exhibited average grain size 200 ± 20 nm and with clear grain boundary which was also substantiated by AFM study. EDX spectrum shows the presence of Bi, La, Ti and O elements in the ceramic. The atomic percentage is inconsistent with stoichiometric of BLTO ceramic which confirms the purity of synthesized BLTO ceramic. Root mean square roughness and average roughness of the ceramic were found to be 58.661 and 46.015 nm, respectively. The presence of blocking and Neel's tempearture in the BLTO ceramic explain the biomodal particle size distribution. Frequency dependent dielectric studies show the low frequency relaxation is associated with the entity of barrier layers at the electrode and the high frequency region with the entity of barrier layers at grain boundaries.